JOURNAL OF MATERIALS SCIENCE 21 (1986) 1479–1486

# Concentration profiles of non-Fickian diffusants in glassy polymers by Rutherford backscattering spectrometry

PETER J. MILLS, CHRISTOPHER J. PALMSTRØM, EDWARD J. KRAMER
*Department of Materials Science and Engineering and Materials Science Center, Cornell University, Ithaca, New York 14853–1501, USA*

Rutherford backscattering spectrometry (RBS) is used to determine the concentration profile of 1,1,1-trichloroethane (TCE) as it diffuses into a crosslinked polymethylmethacrylate (PMMA) glass. The penetration characteristics are those of Case II diffusion, i.e. a diffusion front moves into the glass at a velocity that is roughly constant. Due to the excellent depth resolution (< 30 nm) and sensitivity (< 500 p.p.m. Cl) of RBS the details of the front can be observed. Behind the front where the concentration $\varphi$ of TCE is high and the PMMA is plasticized to a rubbery state, the concentration gradient of TCE is negligible, indicating that the diffusion coefficient of TCE in this region is greater than $10^{-9}\,cm^2\,sec^{-1}$. At the front the concentration of TCE decreases abruptly in less than 100 nm to a lower concentration $\varphi_0$, and subsequently decays exponentially with the distance $x$ from the front. These results are consistent with the Fickian solution to diffusion ahead of a moving boundary, i.e. $\varphi(x) = \varphi_0 \exp[-(vx/D)]$, where $v$ is the velocity of the front and $D$ is the (Fickian) diffusivity of the TCE in the glass ahead of the front. These observations are in qualitative agreement with the predictions of a model of Case II diffusion by Thomas and Windle, and a simplified version of their model is proposed.

## 1. Introduction

Evidence of the non-Fickian nature of the diffusion of organic penetrants into polymer glasses began to emerge more than 30 years ago when the sorption kinetics of organic vapours into these materials was first investigated [1]. Gravimetric experiments in which a polymer sheet was exposed to the penetrant vapour revealed not the $t^{1/2}$ kinetics predicted by the solution to Fick's second law, but rather a weight gain increasing linearly with time. This type of non-Fickian diffusion was first called Case II diffusion by Alfrey [2, 3]; his nomenclature, though non-descriptive, has been adopted by all workers in the field.

Optical microscopic analyses of such sheets have revealed a front at which the penetrant concentration drops sharply. Behind this front the polymer is essentially rubbery, the polymer molecules are oriented normal to the front and the penetrant concentration gradient is thought to be small. After an induction period the front is observed to advance with almost constant velocity, accounting for the linear weight gain with time [2, 7]. The careful gravimetric experiments of Hopfenberg, Stannett, Berens and coworkers [4–12] have revealed the temperature and activity dependence of the front velocity as well as the range of conditions over which Case II diffusion is observed [13].

While gravimetric measurements can be analysed to obtain the front velocity and equilibrium sorption, they cannot yield a detailed description of the concentration profile at the front. Optical [9, 14–17] and radiographic [18] methods used previously had multimicrometre resolution; the concentration profiles obtained by these techniques are thus rather coarse-grained. New techniques with better depth resolution are required to fully reveal these profiles. To this end we have adapted Rutherford backscattering spectrometry (RBS), widely used to depth-profile metals and semiconductors, for use in polymers. This method has the advantages of high sensitivity (< 50 p.p.m. for high $Z$ elements), ease of quantitation and a depth resolution of better than 30 nm. Useful spectra can be obtained in less than 10 min irradiation time and a wide variety of samples may be accommodated. In what follows we outline the essential aspects of this method and demonstrate that the high-resolution concentration profiles of the Case II diffusion front yield new insights into the mechanisms of this mode of diffusion.

## 2. Experimental methods

The diffusion experiments were carried out on a commercial dry-film photoresist, Riston,™ manufactured by DuPont. The 60 $\mu$m thick resist was crosslinked with UV irradiation. The resist has a $T_g$ just below 60° C and its nominal chemical composition as determined by RBS is close to that of polymethylmethacrylate (PMMA). The resist was bonded to a thin copper foil, which in turn was attached to a 1 mm thick aluminium sheet with epoxy adhesive.

0022–2461/86 $03.00 + .12 

1,1,1-Trichloroethane (TCE) was used as the diffusing species for these experiments. When sorbed to equilibrium, it depressed the $T_g$ of the crosslinked resist to or below the ambient temperature, a condition thought to be necessary for Case II diffusion. In addition the three chlorine nuclei in the molecule are good heavy-nuclear "tags", the concentration depth profile of which may be determined using RBS. While the diffusion of TCE was found to be influenced strongly by small-molecule additives [19], the experiments reported here used only one batch of TCE so that the additive content was constant.

Small coupons (17 mm × 17 mm) of the resist on its aluminium backing were immersed in TCE at temperatures between 0 and 40° C. After various times they were taken from the liquid, quickly blown dry with $N_2$ gas and then immediately plunged below the surface of a liquid nitrogen bath. The one-second $N_2$ gas blast removed any excess TCE droplets from the surface. The samples were held in this bath until they were analysed using RBS.

To transfer the cold samples into the RBS analysis chamber the following procedure was adopted. To prevent water condensation on the sample surface during the transfer, the liquid-nitrogen bath is placed in a glove bag which is filled with dry nitrogen. The samples are attached under the liquid nitrogen to a copper mounting block which is screwed on to the end of a rod. Using the rod the block may be inserted into an airlock, which is then evacuated. A gate valve is then opened to allow the block to be inserted on to a dovetail mount on the specimen analysis stage. The rod may be unscrewed from the block and withdrawn, permitting the gate valve to be closed thus isolating the analysis chamber. The specimen analysis stage is cooled by liquid nitrogen flowing through a chamber behind the stage. The stage is surrounded by a liquid-nitrogen cooled shield to prevent condensation of residual vapours in the vacuum system on the sample.

Cooling the sample to liquid-nitrogen temperatures actually has two purposes. The first is to freeze the diffusion profile that was present at the instant the sample was removed from the TCE bath. The sample can then be exposed to the vacuum of the analysis chamber without losing TCE by evaporation from the near-surface layers of the polymer. The second reason is more subtle. It turns out that the incident $He^{2+}$ beam causes severe radiation damage in some polymers, and especially in PMMA. Successive RBS spectra taken of this polymer at room temperature show the progressive loss of oxygen from the near-surface region. Such loss is expected since one result of radiation damage in PMMA is known to be cleavage of the ester side chain. The small-molecule fragments thus produced can diffuse to the sample surface and evaporate. In contrast RBS spectra of the polymer taken with liquid-nitrogen cooling reveal no significant loss of oxygen, nor redistribution of solute, between successive spectra. Although radiation damage undoubtedly still occurs, the molecular fragments produced are frozen in place at these low temperatures and thus the nuclear composition depth profiles obtained from RBS accurately reflect the nuclear composition depth profiles of the undamaged polymer.

## 3. Rutherford backscattering spectrometry

Fig. 1a shows the geometry of the RBS experiment. An $He^{2+}$ ion beam of energy $E_0$ impinges upon the polymer sample at normal incidence. Some of the $He^{2+}$ ions backscattered by nuclei at, or beneath, the polymer surface are collected by an energy-sensitive detector whose output, number of ions against energy, is displayed on a multichannel analyser. The resulting RBS spectrum contains both nuclear composition and depth information.

The nuclear composition information is a result of the influence of the mass of the target nucleus on the energy of the scattered $He^{2+}$ ion. If a nucleus of mass $M$ is at the sample surface the $He^{2+}$ with mass $m$ will be backscattered with an energy $E$ given by

$$E = KE_0 \tag{1}$$

From conservation of momentum and energy [20] it can be shown that for a scattering angle of 180° the kinematic factor $K$ is

$$K = \left(\frac{m - M}{m + M}\right)^2 \tag{2}$$

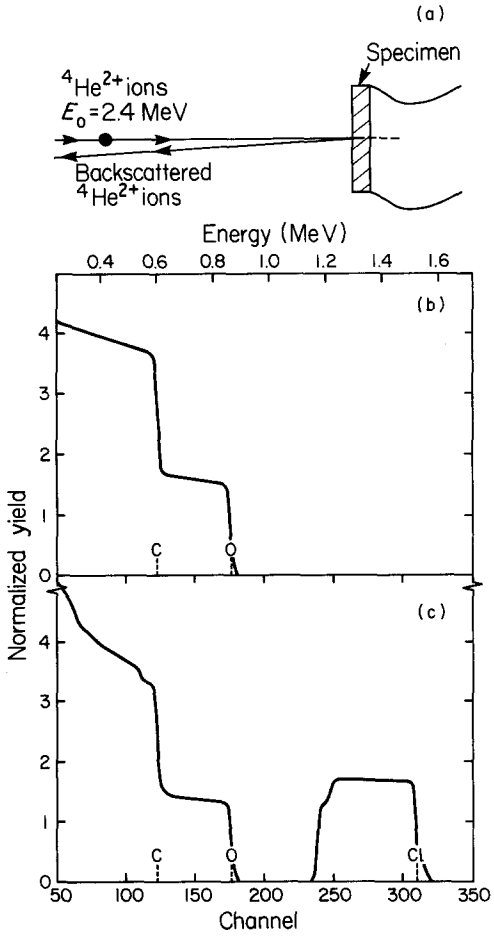


*Figure 1* (a) Geometry of the RBS experiment. (b) Simulated RBS spectrum from 60 μm thick Riston photoresist. (c) Simulated RBS spectrum from 60 mm thick Riston photoresist with a 1 mm thick layer at the surface swollen with TCE to a uniform concentration of 0.1 TCE molecules per PMMA monomer. The energies of $He^{2+}$ ions scattered from chlorine, oxygen and carbon nuclei at the surface of the resist are marked.

For example $^{35}Cl$ has a kinematic factor of 0.632, $^{18}O$ has a $K$ of 0.36 and $^{12}C$ has a $K$ of 0.25. A thin film ($< 50$ nm) has an RBS spectrum consisting of a series of peaks at values of $E$ corresponding to the $K$ values of the nuclei in the film. The areas under such peaks will be proportional to the differential cross-section for Rutherford scattering, $\sigma$. The cross-section is given [20] by

$$\sigma = \left(\frac{e^2 zZ}{4E_0}\right)^2 \left[\frac{\sin^{-4}\theta}{2} - 2\left(\frac{m}{M}\right)^2 + \ldots\right] \quad (3)$$

where $z$ and $Z$ are the atomic numbers of the helium and target nucleus, respectively, and $\theta$ is the angle between the incident and scattered $He^{2+}$ ion beam. The increase in $\sigma$ with $Z^2$ means that RBS is most sensitive to high-$Z$ elements.

In a thick film the $He^{2+}$ ion loses energy to inelastic collisions with electrons as it penetrates the sample. Although these collisions do not produce significant deviations in the direction of the $He^{2+}$ ion, ions backscattered from a nucleus a distance $X$ below the surface will emerge with less energy than those scattered from the surface. The energy loss of the ion may be computed from its stopping cross-section in the target defined by

$$\varepsilon(E) = N^{-1}\frac{dE}{dX} \quad (4)$$

where $N$ is the atomic density of the target. The detailed steps for computing $\varepsilon(E)$ and $dE/dX$ for compounds are given in the literature [20–23]. Using the computed values of $dE/dX$, the energy scale in the RBS spectrum can be converted into a depth scale. Typical values for polymers are about 2 nm per keV at normal incidence. From the usual detector resolution of 16 keV, the depth resolution for polymers is about 30 nm at normal incidence. This resolution may be improved by more than a factor of three by rotating the sample (increasing the angle between the incident beam and the sample normal).

Using the analysis scheme outlined above and given in more detail elsewhere [20, 23], a computer program has been written [24] which will simulate the RBS spectrum to be expected for a certain composition depth profile of the sample. Fig. 1b shows the simulated RBS spectrum from a thick film of PMMA at $E_0 = 2.4$ MeV. The steps in the spectrum correspond to scattering from oxygen and carbon nuclei at the surface of the sample. Fig. 1c shows the simulated RBS spectrum from a thick film of PMMA into which TCE has penetrated to a depth of 1 $\mu$m. The concentration of TCE in the swollen layer is uniform in depth at 0.1 TCE molecules per PMMA monomer, thereby simulating the rubbery layer supposed to form behind the Case II diffusion front. The TCE concentration falls discontinuously to zero at a depth greater than 1 $\mu$m. The chlorine nuclei in the TCE backscatter $He^{2+}$ ions with energies between 1.20 and 1.55 MeV. The steps at the high- and low-energy edges of the chlorine portion of the RBS spectrum are due to the presence of two isotopes of chlorine, $^{35}Cl$ and $^{37}Cl$. If the layer swollen with TCE is made thicker, the low-energy edge of the chlorine portion of the RBS spectrum extends to lower energies but the shape remains similar. A chlorine-containing layer as thick as 1.9 $\mu$m can be analysed by RBS with a 2.4 MeV $He^{2+}$ ion beam without the scattering from chlorine deep in the layer overlapping the scattering from oxygen at the surface of the polymer. While the range of analysis could be increased modestly by increasing the incident beam energy above 2.4 MeV, that energy is approximately the highest energy at which the $He^{2+}$ backscattering cross-sections from the light elements carbon and oxygen are given accurately by the Rutherford formula of Equation 3.

## 4. Results

Fig. 2 shows the RBS spectrum from the photoresist after exposure to TCE for 800 sec at 20.5° C. The

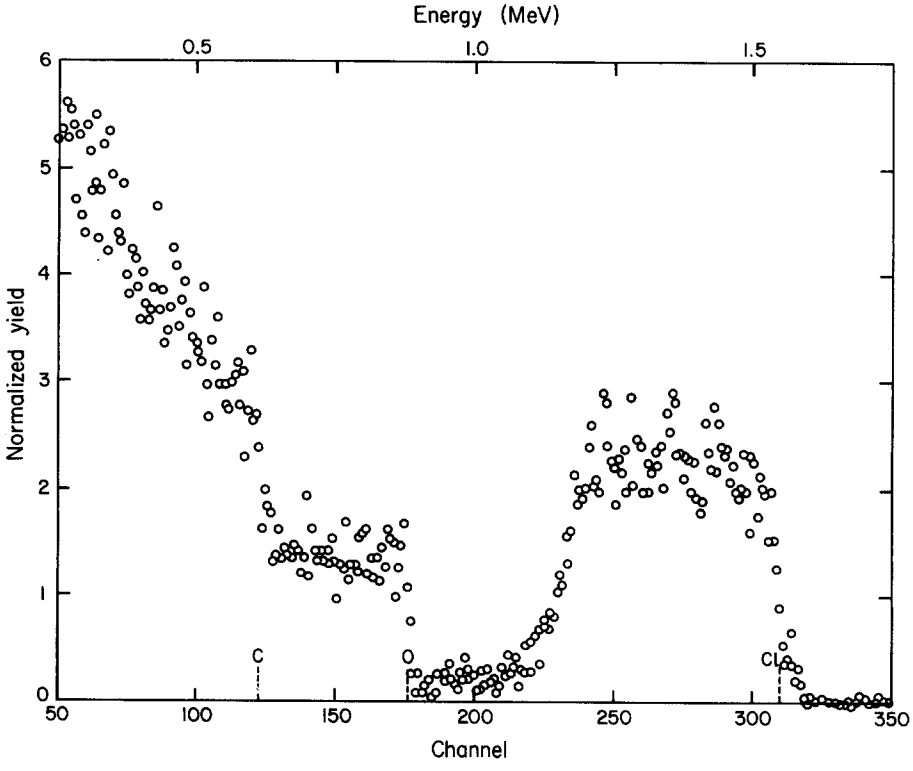


*Figure 2* Experimental RBS spectrum from photoresist after exposure to TCE for 800 sec at 20.5° C. The energies of $He^{2+}$ ions scattered from chlorine, oxygen and carbon nuclei at the surface of the resist are marked.

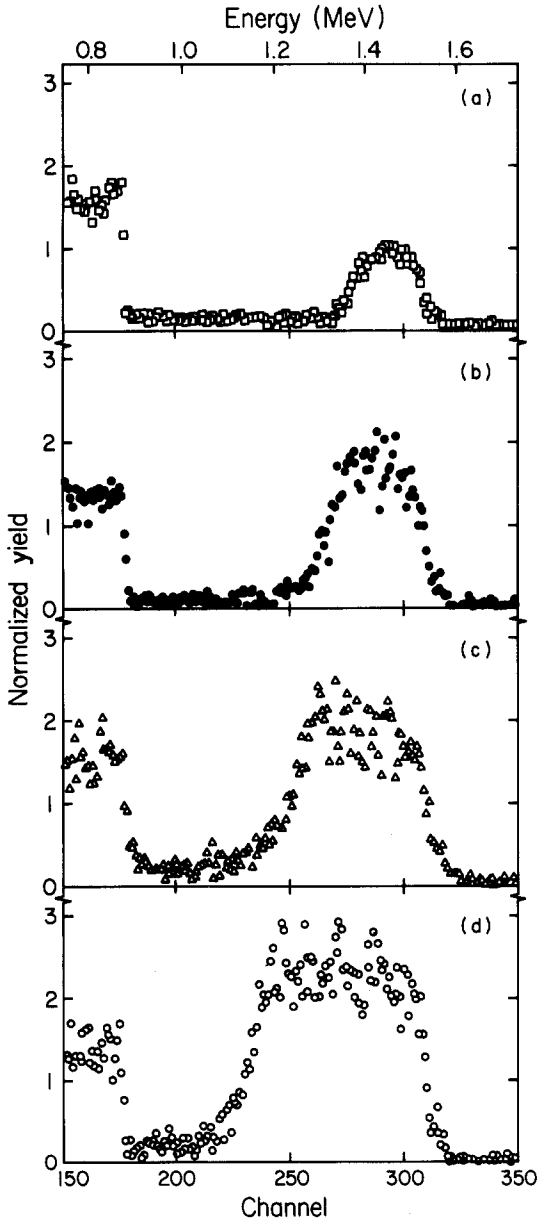


*Figure 3* Experimental RBS spectra from photoresist after exposure to TCE at 20.5° C for the following times: (a) 200, (b) 400, (c) 600, (d) 800 sec.

energies at which $He^{2+}$ ions would be backscattered from chlorine, oxygen and carbon nuclei at the surface are marked. At these energies there are steps which are due to the oxygen and carbon in the polymer and the carbon and chlorine in the absorbed TCE, just as predicted by the simulated spectra in Fig. 1c. Note that the RBS spectrum due to the chlorine appears very similar to that simulated from a layer of constant composition, except that the scattering at the lower-energy edge of this region in the experimental spectrum does not decrease to zero as abruptly as the simulated curve would predict. Nevertheless the decrease in composition ahead of the "front" occurs over a very short distance, certainly much less than 1 $\mu$m

To show that the kinetics of the TCE diffusion are those typical of Case II diffusion it is necessary to record RBS spectra from polymer exposed to TCE for different periods of time. Fig. 3 shows four such spectra from samples of the resist that had been exposed to TCE for 200, 400, 600 and 800 sec. The lower-energy edge of the chlorine RBS spectrum moves progressively to lower energies as the exposure time is increased. Since the energy–depth curve is almost linear over this range, Fig. 3 indicates that the velocity of the front is approximately constant. The depth of the front below the surface can be determined more exactly by finding the thickness of the TCE-rich layer that produces a simulated RBS spectrum that best fits the experimental spectrum. Fig. 4a shows a plot of the front position as a function of time determined from the RBS spectra in Fig. 3.

The TCE concentration behind the Case II front in the sample in Fig. 3 is plotted as a function of time in Fig. 4b. This concentration is determined by matching the yields of the simulated and the observed RBS spectra over the energy range corresponding to the depth of this layer. The concentration of TCE in the layer initially increases with exposure time but then reaches an approximately constant value. There is thus an induction time before the equilibrium surface concentration of TCE is established. Once this induction time has elapsed, the concentration in the region behind the front remains almost constant with time.

RBS spectrometry can also be used to follow the effects of temperature on the Case II diffusion of TCE into the photoresist. Fig. 5 shows three RBS spectra of polymer exposed to TCE. The first was exposed for 10 000 sec at 1.5° C, the second for 600 sec at 20.5° C and the third for 60 sec at 36° C. Spectra obtained as a function of time at these various temperatures reveal similar characteristics to those shown in Fig. 3, i.e. the front velocity $v$ and the concentration $\varphi_\infty$ of TCE

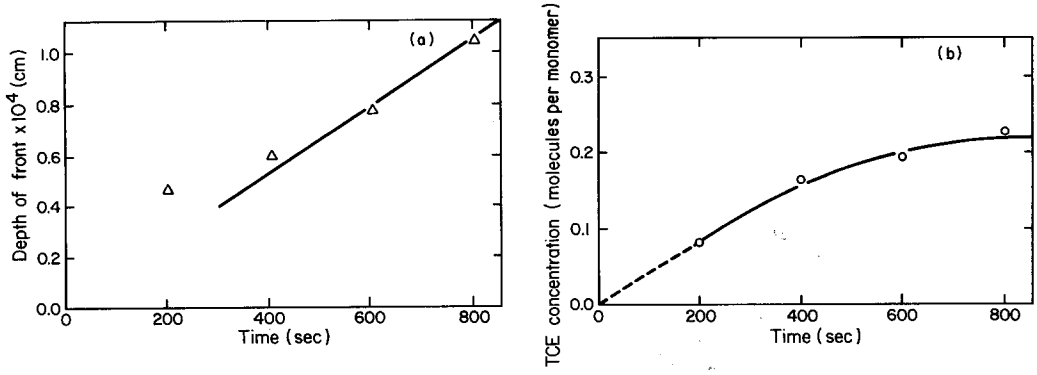


*Figure 4* (a) Depth of Case II diffusion front below the surface as a function of exposure time. (b) Concentration of TCE in the swollen layer behind the front as a function of exposure time. Data are taken from the spectra in Fig. 3.

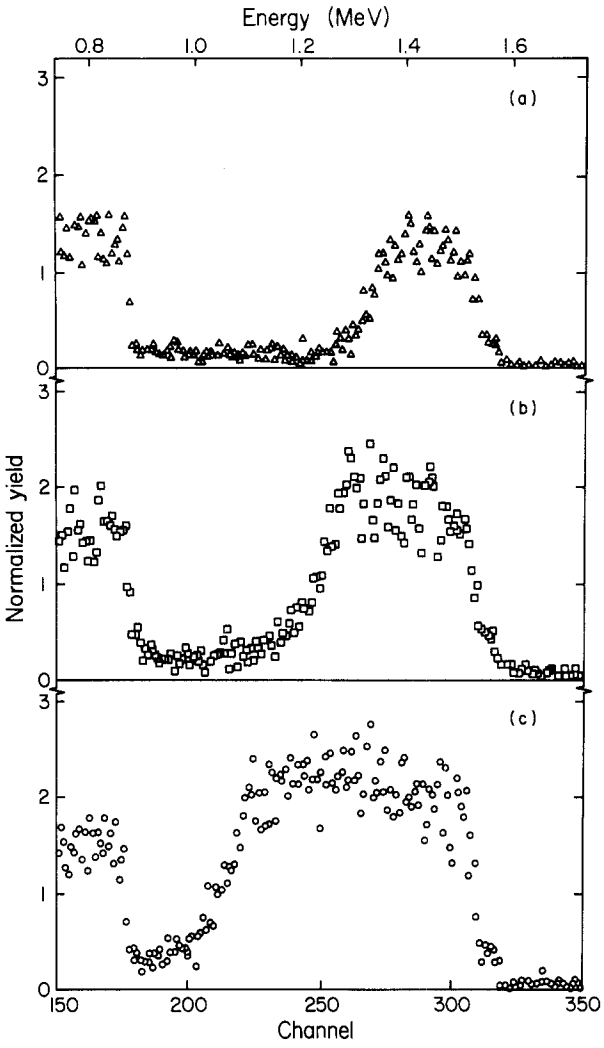


*Figure 5* Experimental RBS spectra from the photoresist exposed to TCE at different temperatures: (a) 1.5° C for 10 000 sec; (b) 20.5° C for 600 sec; (c) 36° C for 60 sec.

behind the front are roughly constant after an initial induction time has elapsed. While $\varphi_\infty$ is rather insensitive to temperature, the values of $v$ extracted from the RBS data increase markedly with increasing temperature. This velocity is thermally activated, as shown by the Arrhenius plot in Fig. 6 whose slope corresponds to an effective activation enthalpy for $v$ of 115 KJ mol$^{-1}$ or 1.19 eV.

## 5. Discussion

While various models for the Case II diffusion process have been proposed [25–40], it now seems clear that some coupling between the mechanical response of the polymer to swelling and diffusion is required. Based on the RBS measurements of the concentration–depth profiles we can test some of these models. Wang and co-workers [31, 32] suggested that the front velocity was controlled by convective transport of solute due to a gradient in its partial stress tensor. As pointed out by Peterlin [33–35], however, this model implies the development of a significant concentration gradient of solute behind the front. All our observations of the TCE concentration–depth profiles show just the opposite. The concentration gradient of TCE is negligible behind the front. Since we have determined that this swollen polymer layer is rubbery in supplemental experiments, the absence of a gradient is not astonishing. For the exposure times used the absence of a resolvable diffusional concentration gradient over the small distances profiled behind the front is consistent with a diffusion coefficient of TCE greater than $10^{-9}$ cm$^2$ sec$^{-1}$. Such values are typical for the diffusion of molecules the size of TCE into rubbery networks [41].

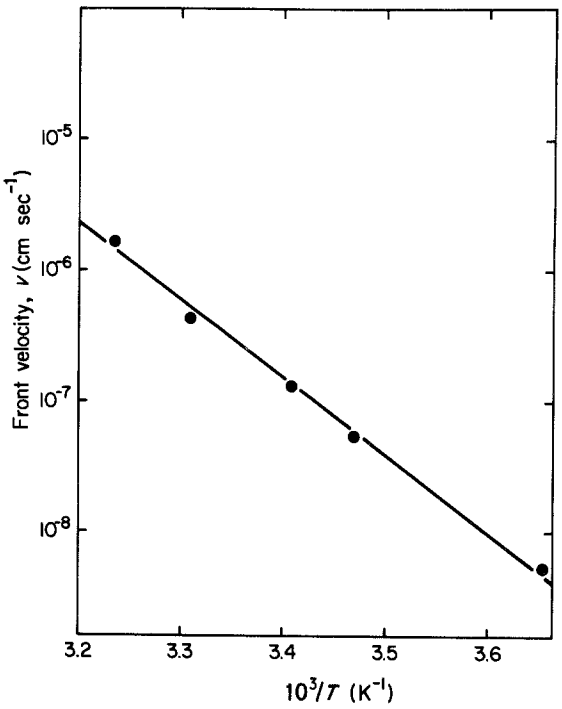


*Figure 6* Logarithm of the Case II front velocity plotted against the reciprocal of the absolute temperature.

Peterlin [33–35] proposed that the front was preceded by a Fickian diffusion precursor up to a concentration $\varphi_0$ where the swelling stresses are sufficient to break chains in the glass, at which point the concentration increases to its higher value $\varphi_\infty$ in the rubbery state. Without passing judgement at this time on the merits of his proposal that the front velocity is controlled by network chain scission, we can test his hypothesis of the existence of a Fickian precursor. The problem is one of diffusion ahead of a moving boundary. The steady-state solution, obtained after the front has moved several characteristic lengths of the precursor [42], is given by

$$\varphi(x) = \varphi_0 \exp\left(\frac{-vx}{D}\right) \quad (5)$$

where $v$ is the front velocity, $x$ is the distance ahead of the moving front and $D$ is the diffusion coefficient of the TCE in the glass ahead of the front. Fig. 7a shows schematically the expected diffusion profile. Since we measure $\varphi$, $v$ and $x$ directly by RBS we can test Equation 5, and if valid, use it to extract values of $D$ from our data.

Fig. 7b shows the RBS spectrum from the polymer exposed to TCE for 800 sec at 20.5° C. A simulated RBS spectrum is shown by the solid line [43]. This spectrum was derived from a concentration–depth profile predicted by Equation 5 using the experimental front velocity of 1.4 nm sec$^{-1}$, the measured $\varphi_0$ of 0.09 TCE molecules per PMMA monomer, and a $D$ of 3 ×

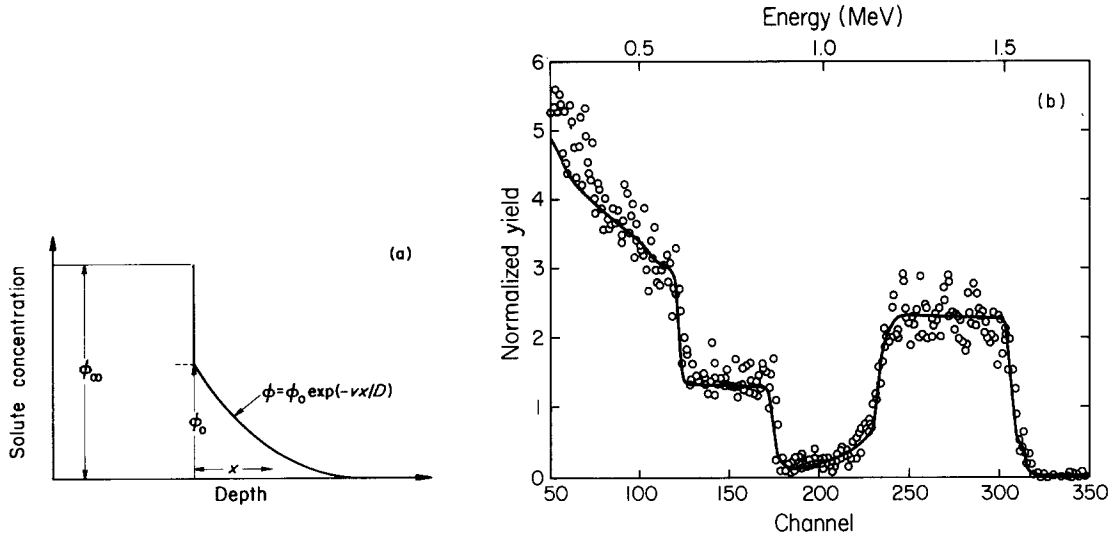


*Figure 7* (a) Expected TCE concentration profile for Case II diffusion. (b) Simulated RBS spectrum (solid line) from the TCE concentration profile in (a) using the measured front velocity $v = 1.4\,\text{nm sec}^{-1}$ at 20.5° C, $\varphi_0 = 0.09$ TCE molecules per PMMA monomer, and $D = 3 \times 10^{-12}\,\text{cm}^2\,\text{sec}^{-1}$. The fit to the experimental spectrum (open circles) is good.

$10^{-12}\,\text{cm}^2\,\text{sec}^{-1}$. The fit is very good. Fits of similar quality were obtained for all experimental conditions investigated. The precursor seems to be well described by Fickian diffusion kinetics with a $D$ that is approximately independent of solute concentration $\varphi$, at least up to $\varphi_0$.

A fitting procedure similar to the one above was used to extract $D$ (for TCE diffusion ahead of the front) from the other RBS spectra. After the front had progressed at least 0.6 $\mu$m from the surface of the polymer, i.e. after the induction period, the measured values of $D$ were approximately independent of time and front position. The values, ranging from $2 \times 10^{-11}\,\text{cm}^2\,\text{sec}^{-1}$ at 36° C to $7 \times 10^{-14}\,\text{cm}^2\,\text{sec}^{-1}$ at 1.5° C, are shown on an Arrhenius plot in Fig. 8. The slope of this plot corresponds to an activation enthalpy of $115\,\text{KJ mol}^{-1}$ or 1.19 eV. This activation enthalpy is in remarkable agreement with that

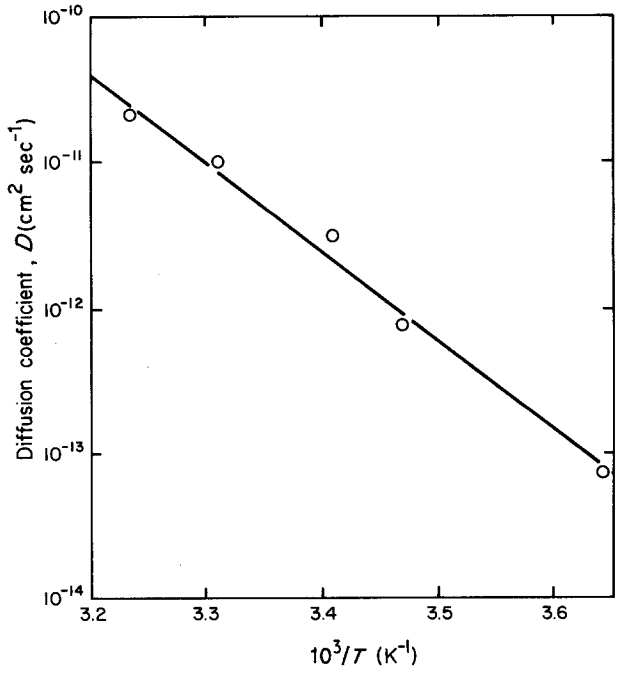


*Figure 8* Logarithm of the diffusion coefficient of TCE in the glassy photoresist against reciprocal of the absolute temperature.

obtained from the temperature dependence of the front velocity, reflecting the fact that the spatial extent of the precursor diffusion, which scales as $D/v$, is roughly independent of temperature over a range where the velocity is changing by over two orders of magnitude.

While the Peterlin proposal of a Fickian precursor certainly seems to be verified, his idea that the front velocity is controlled by chain scission of the network seems unlikely. It is difficult to see why, for example, such chain scission control should give rise to the induction period, demonstrated in Fig. 4, in which the surface solute concentration falls well below the equilibrium concentration. More recent papers have emphasized the role of the osmotic pressure developed as a result of the glacially slow relaxation of the polymer glass toward a true equilibrium swollen state [36–40]. Since the relaxation time of the polymer decreases greatly as the concentration of solute increases due to plasticization, a rapid increase in the rate of swelling, $\mathrm{d}\varphi/\mathrm{d}t$, can occur after a certain concentration is reached, resulting in principle in a sharp front.

In the most highly developed of these models, that of Thomas and Windle [40], the swelling rate is treated as the rate of linear viscoelastic deformation driven by the osmotic pressure. Their numerical simulation of the coupled swelling–diffusion problem revealed that a front forms, the velocity of which is controlled by the value at the front of $(D\,\mathrm{d}\varphi/\mathrm{d}t)^{1/2}$. The swelling rate of an element of the molecular network ahead of the front is given by

$$\frac{\mathrm{d}\varphi}{\mathrm{d}t} = \frac{P}{\eta} \tag{6}$$

where $P$ is an osmotic pressure that drives the swelling and may be approximated as

$$P = \frac{k_B T}{\Omega} \ln\left(\frac{\varphi_{eq}}{\varphi}\right) \tag{7}$$

where $\Omega$ is the partial molecular volume and $\varphi_{eq}$ is a solute concentration in local equilibrium. The volumetric viscosity $\eta$ is assumed to decrease exponentially

with $\varphi$ to simulate the decrease in polymer relaxation time due to plasticization, i.e.

$$\eta = \eta^* \exp(-M\varphi) \quad (8)$$

As one approaches the front from the glass, from large $x$ toward smaller $x$ in Fig. 7a, there will be a region where $P$ increases (osmotic pressure builds up), reaches a maximum, and then decreases (osmotic pressure decays) as $\eta$ decreases with increasing $\varphi$. To proceed further we assume a steady-state activity gradient ahead of the front, i.e.

$$\varphi_{eq}(x) = \varphi_{eq\infty} \exp\left(\frac{-vx}{D^T}\right) \quad (9)$$

where $\varphi_{eq\infty}$ is the solute concentration in equilibrium in the rubbery region and $D^T$ is a diffusion coefficient which would characterize the concentration gradient if $P = 0$ (local equilibrium). From Equation 7 we can derive the following expression for the osmotic pressure gradient:

$$\frac{dP}{dx} = -\frac{k_B T}{v\Omega}\left(\frac{v^2}{D^T} - \frac{d(\ln\varphi)}{dt}\right) \quad (10)$$

The region of osmotic pressure build-up is where $d(\ln\varphi)/dt < v^2/D^T$, whereas the region of osmotic pressure decay is where $d(\ln\varphi)/dt > v^2/D^T$. Since at steady state the $x$ position, $x_0$, of the pressure maximum must be constant, the front velocity is given by

$$v = \left(D^T d\frac{(\ln\varphi_m)}{dt}\right)^{1/2} \quad (11)$$

where $d(\ln\varphi_m)/dt (= \varphi_m^{-1} dr_m/dt)$ is evaluated at the osmotic pressure maximum. This expression has the same form as the numerical results of Thomas and Windle [40]. To proceed further we can assume that $D^T \approx D$ and that the position of the pressure maximum is just ahead of the front so that $\varphi_m = \varphi_0$. Substituting the swelling rate from Equation 6 we find

$$v = \left(D\frac{P_0}{\eta_0\varphi_0}\right)^{1/2} \quad (12)$$

where $P_0$ and $\eta_0$ are the values of osmotic pressure and viscosity at $\varphi_0$. Before a steady state can be achieved an induction time for swelling must be exceeded. This time $t_i$ is approximately given by

$$t_i \approx \frac{\eta_0}{MP_0} \quad (13)$$

Even this simplified version of the Thomas and Windle model is difficult to test completely with the present data. We will content ourselves here with pointing out some qualitative correspondences and some obvious discrepancies. An induction period where $\varphi$ falls below its equilibrium value at the surface is predicted and observed. Future experiments must however be carried out to test whether Equations 5 to 7 quantitatively describe the kinetics of the approach to equilibrium.

Intuitively we expect that the polymer at the front is plasticized so that $T_g$ has been reduced to not much above the ambient temperature. Clearly therefore $\varphi_0$ should decrease with increasing ambient temperature. Although the uncertainty in $\varphi_0$ is relatively large, we find that $\varphi_0$ decreases from 0.1 TCE molecules per monomer at 1.5° C to 0.07 TCE molecules per monomer at 36° C. Over the same range of temperature $\varphi_\infty$ increases from 0.13 to 0.27 TCE molecules per monomer.

Since we expect $P_0 \approx (k_B T/\Omega)\ln(\varphi_\infty/\varphi_0)$ we can compute the value of $\eta_0$ from Equation 12. The resulting values decrease with increasing temperature and fall in the range $10^{13}$ to $10^{10}$ poise, reasonable magnitudes for the viscosity near $T_g$. If we take literally the idea that $\varphi_0$ decreases $T_g$ to room temperature, $\eta_0$ should be independent of temperature. Following that thought further we see from Equation 12 that $v$ should be much less temperature-dependent than $D$, i.e. the activation enthalpy for the front velocity should be about half that for diffusion in the glass. The data reported above show these two activation enthalpies to be approximately equal. While we expect that some of the discrepancy may arise from the presence of additives in the TCE that diffuse faster than TCE into the glass and "preplasticize" it [43], it seems clear that the simple model can not account for all aspects of Case II diffusion. It is equally clear, however, that the detailed knowledge of the local solute concentrations in the neighbourhood of the front, available for the first time using RBS analysis, will allow us to rapidly test and develop improved models of the Case II diffusion process in the future.

## Acknowledgements

The support of this research by IBM is gratefully acknowledged. Partial support for one of us (P.J.M.) was provided by the Cornell Materials Science Center, which is funded by the DMR–MRL program of NSF. The research would have been impossible without the guidance and enthusiastic advice on all aspects of the ion-beam analysis from Professor J. W. Mayer. We also appreciate useful discussions with A. Windle, R. Lasky, G. Jones and P. Issacs.

## References

1. J. CRANK and G. S. PARK, *Trans. Faraday Soc.* **82** 1072 (1951).
2. T. ALFREY, *Chem. Eng. News* **43** (1965) 64.
3. T. ALFREY, E. F. GURNEY and W. G. LLOYD, *J. Polym. Phys. C.* **12** (1966) 249.
4. H. B. HOPFENBERG, R. H. HOLLEY and V. STANNETT, *Polym. Eng. Sci.* **9** (1969) 242.
5. R. H. HOLLEY, H. B. HOPFENBERG and V. STANNETT, *ibid.* **10** (1970) 376.
6. B. R. BAIRD, H. B. HOPFENBERG and V. STANNETT, *ibid.* **11** (1971) 274.
7. C. H. M. JACQUES, H. B. HOPFENBERG and V. STANNETT, *ibid.* **13** (1973) 81.
8. C. H. M. JACQUES and H. B. HOPFENBERG, *ibid.* **14** (1974) 441.
9. L. NICOLAIS, E. DRICOLI, H. B. HOPFENBERG and D. TIDONE, *Polymer* **18** (1977) 1137.
10. A. R. BERENS and H. R. HOPFENBERG, *ibid.* **19** (1978) 489.
11. D. J. ENSCORE, H. B. HOPFENBERG, V. STANNETT and A. R. BERENS, *ibid.* **18** (1977) 1105.
12. A. R. BERENS and H. R. HOPFENBERG, in "Structure and Properties of Amorphous Polymers," edited by A. G. Walton (Elsevier, Amsterdam, 1978) p. 77.

13. H. R. HOPFENBERG and H. L. FRISCH, *J. Polym. Sci., Poly. Lett.* **7** (1969) 405.
14. N. L. THOMAS and A. H. WINDLE, *Polymer* **18** (1977) 1195.
15. *Idem, J. Membrane Sci.* **3** (1978) 337.
16. *Idem, Polymer* **21** (1980) 619.
17. *Idem, ibid.* **22** (1981) 627.
18. F. A. LONG and D. RICHMOND, *J. Amer. Chem. Soc* **82** (1960) 513.
19. P. J. MILLS and E. J. KRAMER, unpublished work.
20. W. -K. CHU, J. W. MAYER and M. -A. NICOLET, in "Backscattering Spectrometry" (Academic Press, New York, 1978) p. 2.
21. J. F. ZIEGLER, (ed.) in "The Stopping and Ranges of Ions in Matter," Vol. 4 (Pergamon Press, New York, 1977).
22. H. H. ANDERSON and J. F. ZIEGLER, "The Stopping and Ranges of Ions in Matter", Vol. 3 edited by J. F. Ziegler (Pergamon Press, New York, 1977).
23. J. F. ROMANELLI, J. W. MAYER, E. J. KRAMER and T. P. RUSSELL, *J. Polym. Sci. Polym. Phys.*, in press.
24. L. DOOLITTLE, *Nucl. Inst. Methods* **B93** (1985) 344.
25. J. CRANK, *J. Polym. Sci.* **11** (1953) 151.
26. G. S. PARK, *ibid.* **11** (1953) 97.
27. E. BAGLEY and F. A. LONG, *J. Amer. Chem. Soc.* **77** (1955) 2172.
28. A. C. NEWNS, *Trans. Faraday Soc.* **52** (1956) 1533.
29. R. A. WARE and C. COHEN, *J. Appl. Polym. Sci.* **25** (1980) 717.
30. R. A. WARE, S. TIRTOWIDJOJO and C. COHEN, *ibid.* **26** (1981) 2975.
31. H. L. FRISCH, T. T. WANG and T. K. KWEI, *J. Polym. Sci. A2* **7** (1969) 872.
32. T. T. WANG, T. K. KWEI and H. L. FRISCH, *ibid.* **7** (1969) 2019.
33. A. PETERLIN, *J. Polym. Sci.* **3** (1965) 1083.
34. *Idem, Makromol. Chem.* **124** (1969) 136.
35. *Idem, J. Res. NBS* **81A** (1977) 243.
36. J. H. PETROPOLIS and P. P. ROUSIS, *J. Chem. Phys.* **47** (1967) 1491.
37. *Idem, J. Polymer Sci. C* **22** (1969) 917.
38. J. H. PETROPOLIS, *J. Polymer Sci., Polym. Phys.* **22** (1984) 183.
39. G. SARTI, *Polymer* **20** (1979) 827.
40. N. L. THOMAS and A. H. WINDLE, *ibid.* **23** (1982) 529.
41. G. S. PARK, in "Diffusion in Polymers", edited by J. Crank and G. S. Park (Academic Press, London, 1968) p. 114.
42. H. S. CARSLAW and J. C. JAEGER, in "Conduction of Heat in Solids" (Oxford University Press, 1959) p. 373.
43. P. J. MILLS and E. J. KRAMER, unpublished work.

*Received 8 May*
*and accepted 12 June 1985*